Magnetic resonance imaging after radiofrequency ablation in a rodent model of liver tumor: tissue characterization using a novel necrosis-avid contrast agent

Yicheng Ni
Feng Chen
Stefaan Mulier
Xihe Sun
Jie Yu
Willy Landuyt
Guy Marchal
Alfons Verbruggen

Y. Ni (✉) · F. Chen · S. Mulier ·
X. Sun · J. Yu · G. Marchal
Department of Radiology,
University Hospitals,
Catholic University of Leuven,
Herestraat 49,
3000 Leuven, Belgium
e-mail: Yicheng.Ni@med.kuleuven.
ac.be
Tel.: +32-16-345940
Fax: +32-16-343765

F. Chen
Department of Radiology,
Zhong Da Hospital,
Southeast University,
Nanjing, Jiangsu,
People's Republic of China

S. Mulier
Department of Surgery,
University Hospital of Mont-Godinne,
Catholic University of Louvain,
Yvoir, Belgium

X. Sun
Department of Radiology,
Affiliated Hospital,
Weifang Medical University,
Weifang, Shandong
People's Republic of China

W. Landuyt
Laboratory of Experimental Oncology,
University Hospitals,
Catholic University of Leuven,
Leuven, Belgium

A. Verbruggen
Laboratory of Radiopharmaceutical
Chemistry,
Faculty of Pharmaceutical Sciences,
Catholic University of Leuven,
Leuven, Belgium

Abstract We exploited a necrosis-avid contrast agent ECIV-7 for magnetic resonance imaging (MRI) in rodent liver tumors after radiofrequency ablation (RFA). Rats bearing liver rhabdomyosarcoma (R1) were randomly allocated to three groups: group I, complete RFA, group II, incomplete RFA, and group III, sham ablation. Within 24 h after RFA, T1-weighted (T1-w) MRI was performed before and after injection of ECIV-7 at 0.05 mmol/kg and followed up from 6–24 h. Signal intensities (SIs) were measured with relative enhancement (RE) and contrast ratio (CR) calculated. The MRI findings were verified histomorphologically. On plain T1-w MRI the contrasts between normal liver, RFA lesion, residual and/or intact tumor were vague. Early after administration of ECIV-7, the liver SI was strongly enhanced (RE=40–50%), leaving the RFA lesion as a hypointense region in groups I and II. At delayed phase, two striking peri-ablational enhancement patterns appeared (RE=90% and CR=1.89%), i.e., "O" type of hyperintense rim in group I and "C" type of incomplete rim in group II. These MRI manifestations could be proven histologically. In this study, tissue components after RFA could be characterized with discernable contrasts by necrosis-avid contrast agent (NACA)-enhanced MRI, especially at delayed phase. This approach may prove useful for defining the ablated area and identifying residual tumor after RFA.

Keywords Contrast media ·
RF ablation · MRI · Necrosis ·
Liver neoplasm · Rat experiment ·
Histology

Introduction

Thermal ablation therapies, including radiofrequency ablation (RFA), interstitial laser thermotherapy (ILT), microwave, cryotherapy, and high-intensity focused ultrasound (HIFU) are minimally invasive or non-invasive alternatives to conventional surgical resection, particularly for the treatment of malignant solid tumors [1, 2]. The term ablation used here refers to sort of virtual surgical ablation, i.e., using either hot or cold thermal energies to coagulate or to devitalize, in situ, the unwanted tissue but without removing it from the patient, resulting in an effect comparable to that of surgical resection [1].

Therefore, early but non-invasive and unequivocal identification and demarcation of the intended tissue coagulation as a common endpoint of all these therapies become clinically crucial for therapeutic assessment. Such information helps to justify the therapeutic decision and optimize

the protocols for each individual patient. For instance, upon timely detection, any part that escaped from initial ablation may regain the chance of eradication through a complementary treatment session.

However, non-enhanced or plain scans at different imaging modalities such as ultrasound (US), computed tomography (CT) and magnetic resonance imaging (MRI) are known to generate only atypical findings of obscurely altered regional echogenicity, density, and signal intensity, respectively, and, therefore, are inaccurate, non-specific and unreliable with respect to clear discrimination between induced coagulation and various adjacent viable tissue components.

With the use of commercial extracellular fluid space (EFS) contrast agents (CAs) for imaging contrast enhancement (CE), CT and MRI are able to demonstrate circumscribed hypodense or non-enhancing regions a few minutes after ablation, reflecting the extent of tissue destruction [3]. In current clinical practice, identification of a previously enhancing tumor but void CE post-therapy is regarded as an early predictor of tumor ablation. Because these EFS CAs equally enhance peri-ablational untreated tumor and benign inflammatory tissues at early stages, the detection of local tumor relapse has to rely on periodical imaging follow-up every 3 to 6 months [4, 5], leaving broad time windows for malignant progression and metastasis and, consequently, unsatisfactory long-term patient survival. Whilst such inadequate specificity of EFS CAs has been generally recognized [3–6], whether the use of macromolecular blood-pool CAs represents a better solution for early differentiation between peri-ablational benign and malignant tissues after RFA is still under discussion [7–9].

Alternatively, the development of necrosis-avid contrast agents (NACAs), which have evolved from porphyrin to non-porphyrin generations [10], might provide a solution to tackle this problem. In addition to necrosis labeling as has been demonstrated for non-invasive imaging assessment of myocardial viability [10–18], other observed multifunctional features, such as blood-pool effect, adrenal and splenic enhancement as well as hepatobiliary and renal dual excretions, may render NACAs as versatile contrast enhancers for various additional applications [10, 19]. The present animal experiment was performed to explore the utility of a representative non-porphyrin NACA, namely bis-Gd-DTPA-bisindole or ECIV-7 [10], for therapeutic assessment of liver tumor after RFA in a rodent liver tumor model.

Materials and methods

Animal model

This animal experiment was in compliance with the current institution regulations for use and care of laboratory animals. Subcutaneously implanted rhabdomyosarcoma (R1)

in rats is one of the most widely used tumor models in cancer research for its biological stability and responsiveness to various therapeutic interventions [20]. Liver implantation of R1 has been established recently [21] and was chosen for the present study. Eighteen male WAG/Rij rats (Iffa Credo, Brussels, Belgium), weighting approximately 320 g were anesthetized with intraperitoneal injection of Nembutal (Sanofi Sante Animale, Brussels, Belgium) at 40 mg/kg and were subjected to midline laparotomy, as tumor recipients. A 2 mm^3 piece of tumor, freshly harvested from a donor rat with subcutaneous growth of R1, was implanted in the left lateral liver lobe of the recipient rat, which was allowed to recover after closure of the abdomen with layered sutures. Being monitored routinely with MRI, the liver R1 tumors were grown to 0.5–0.8 cm within 10 days after implantation, ready to receive the experimental treatments. The details of the liver mass preparation, biological behavior, imaging manifestations, and histopathological features of this R1 tumor model have been introduced elsewhere [21].

Contrast agent

A colorless non-porphyrin NACA, namely ECIV-7 or bis-Gd-DTPA-bisindole chelate, in an aqueous solution of 0.05 mmol/ml gadolinium, was used as a T1 positive contrast enhancer in this study for intravenous bolus injection at a dose of 50 μmol/kg body weight. The chemical structure, synthetic process, physicochemical properties and CE performances of ECIV-7 at MRI relative to the dark-red porphyrin NACA Gadophrin-2 and another light-yellow non-porphyrin NACA ECIII-60 are described in detail elsewhere [10, 22, 23]. This non-porphyrin NACA compound shares general pharmacodynamic behavior with the porphyrin NACA Gadophrin-2, but is apparently devoid of color and phototoxicity as well as stronger in necrosis avidity by displaying both T1 and T2 contrast enhancement on the respective sequences due to accumulation in the reperfused myocardial infarction [10].

Study protocol

Eighteen rats bearing liver R1 tumors were randomly allocated into three groups of six rats each for the subsequent treatments: in group I, with complete RFA (30 W, 30 s), the tumor was coagulated with a 3–5 mm peritumoral margin; in group II, with incomplete RFA (30 W, 20 s), the edge of approximately 25% of the tumor volume was intentionally spared from ablation; in group III, with sham ablation, the rats received all interventions, including anesthesia, open abdominal surgery and electrode insertion, but without the radiofrequency (RF) energy switched on. Within 12 h to 24 h after RFA, to mimic an overnight recovery in clinical patients, contrast-enhanced MRI was performed before and

after intravenous administration of ECIV-7 at early phase every 10 min for the first hour and at delayed phase between 6 h and 24 h after contrast enhancement, according to previous experiences with NACAs [11, 12, 16, 24, 25].

RFA procedure

Under the same anesthesia and laparotomy as in tumor implantation, the liver lobe bearing R1 tumor was exposed out of the incision and held gently by the operator. Being connected to a 500 kHz RF generator (RFG-3E, Radionics, Burlington, Mass., USA), an 18-gauge electrode with a 1 cm uninsulated cool tip was inserted into the middle of the palpable R1 tumor. For conducting this monopolar RFA, the electric circuit was completed through a 10 cm×8 cm metallic grounding pad underneath the shaved back of the rat. Under power control mode (30 W), RF current was delivered into the tumor for approximately 30 s and 20 s in groups I and II, respectively, and was seized depending on experimental needs. Rats in group III received only sham RFA. The abdominal incision in all rats was closed after the treatments.

MR scanning and imaging analyses

Gas anesthesia was applied for MRI. Through a mask connected via a 10 m-long polyethylene tube to an IMS gas anesthesia system (Harvard Apparatus, Holliston, Mass, USA) located outside the MR room, the rat initially inhaled, and was later sustained with, 4% and 2%, respectively, of isoflurane in a mixture of 20% oxygen and 80% room air. The animal was placed in the supine position in a plastic holder with its tail vein cannulated for contrast agent injection [21].

MRI was performed with a four-channel phased array wrist coil (MRI Devices Corporation, Waukesha, Wis., USA) in a 1.5 T whole-body scanner (Sonata, Siemens, Erlangen, Germany) of 40 mT/m maximum gradient capacity. For each imaging sequence 12 transverse images were acquired, with a slice thickness of 2.0 mm gapped at 0.4 mm.

A turbo-spin echo T2-weighted sequence (TSE-T2WI) was used for monitoring tumor growth, with the following acquisition parameters: repetition and echo times (TR/TE) 3,800/100 ms, turbo-factor 19, field of view (FOV) 120 mm× 50 mm, imaging acquisition matrix 256 pixels×104 pixels, and three averages, lasting 1 min and 8 s for one measurement.

Turbo-spin echo T1-weighted imaging (TSE-T1WI) was performed for contrast agent study, with the following acquisition parameters: TR/TE 535/8.6 ms, turbo factor 7, FOV 120 mm×50 mm, matrix 256 pixels×104pixels, two concatenations and four averages, leading to an in-plane resolution of $0.5×0.5$ mm^2 and total scan time of 1min and 12s.

A glass tube containing 0.02% $CuSO_4$ solution was placed beside the rat as an external standard for normalization of signal intensity (SI) values. For different tissue components, including normal liver, coagulated RFA lesion, and residual tumor in groups I and II, and intact liver and tumor in group III, the SIs were measured on all lesion-containing slices, using a circular region of interest (ROI) with 5–80 pixels, by two investigators who were unaware of the study protocol. In the same animal, the size and location of the ROI were kept constant for measurements at different time points. The SI values obtained were normalized, using the formula: $SI_{normalized}=SI_{post}×(SI_{standard\ pre}/SI_{standard\ post})$, and averaged for each group at each time point. The degree of SI enhancement of each tissue was calculated as the relative enhancement (RE), using the formula: $RE\%=(SI_{postcontrast}−SI_{precontrast})/SI_{precontrast}×100$. The visual conspicuity of adjacent tissues on the same image was expressed as contrast ratio (CR) and calculated with the formula: $CR=SI_{tissueA}/SI_{tissueB}$. As a rule, for the use of T1 CAs, the imaging contrasts were defined as the following: there was no contrast when CR equaled nearly 1; negative contrast when 0<CR<1; positive contrast when CR>1; ambiguous-to-weak positive contrast when 1.0<CR<1.2; good positive contrast when 1.2≤CR<1.5; and strong positive contrast when CR≥1.5. Empirically, with the systemic use of NACAs at a dose of 0.05–0.1 mmol/kg, a necrosis-specific CE could be reliably determined only when a value of lesion-over-normal CR above 1.5 was achieved at delayed phase of a few hours persisting to a few days [10–12, 15–18, 24, 25].

Histopathology

At the end of imaging studies all rats were euthanized by intravenous overdose of phenobarbital. To pursue optimal macroscopic and microscopic effects, we carried out the following two different postmortem procedures. Half the rats (n=3) in each group were placed in a deep freezer (−30°C) overnight in the same position as that during MRI. The frozen rats were sectioned with a bone saw (Medoc beta 200, Medoc SA, Pol. Cantabria Logroño, Spain) in the transverse plane similar to that on MRI. The body sections were photographed with a digital camera, to match the macroscopic findings with the corresponding contrast-enhanced MR images, and further processed for microscopy. For the other half of the animals the entire liver was excised and suspended in 10% formalin, for fixation, and later processed for hematoxylin–eosin staining for histological documentation with a camera-ready light microscope (Axioskop 50, Carl Zeiss, Oberkochen, Germany) [21]. Attention was paid during microscopic interpretations
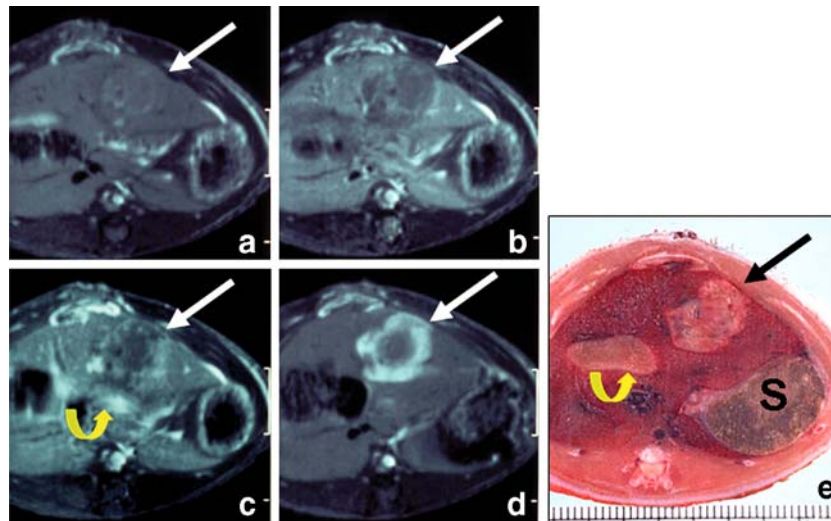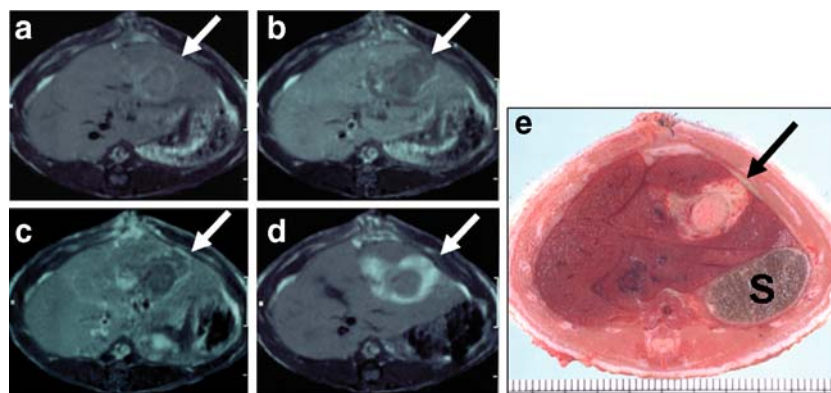
Fig. 1 T1-weighted TSE MR images. **a** before and **b–d** after intravenous injection of a non-porphyrin NACA ECIV–7 at 0.05 mmol/kg and **e** corresponding macroscopic section from a group I rat with liver implantation of R1 tumor and 1 day after complete ablation of the tumor. While hardly discernible before contrast enhancement (**a**), the RFA lesion (*arrow*) was demarcated as a hypointense area 10 min after injection of ECIV–7 (**b**), due to strongly enhanced normal liver. At 40 min after contrast enhancement (**c**), with time, a progressively brightening and concentrically thickening rim occurred at the periphery of the RFA lesion, accompanied by evident biliary contrast excretion, shown as strong CE at the duodenum (*curved arrow*). Twenty-four hours after administration (within the broad imaging window from a few hours to a few days for any NACAs), ECIV-7 caused a typical "O" type of CE pattern (**d**). The tumor as the core of this RFA-induced necrotic lesion was completely encompassed by a thick specifically enhanced rim composed of necrotic periphery, suggesting radical tumor ablation. These imaging findings matched well with the gross section (**e**). *S* stomach

to rule out artificial vacuoles, cracks and deformations caused by the first cryopreservation procedure, which, albeit, yielded satisfactory macroscopic views.

Statistical analysis

Numerical data derived from the same tissue at the same time point were pooled from all groups of animals, as

Fig. 2 T1-weighted TSE MR images. **a** before and **b–d** after intravenous injection of a non-porphyrin NACA ECIV-7 at 0.05 mmol/kg and **e** corresponding macroscopic section from a group I rat with liver implantation of R1 tumor and 1 day after complete ablation of the tumor. While faintly discernible before contrast enhancement (**a**), the RFA lesion (*arrow*) was demarcated as a hypointense area 10 min after injection of ECIV-7 (**b**), due to strongly enhanced normal liver. The shape of the lesion was not spherical due to the "lobectomy" effect resulting from RFA-induced vascular thrombosis at the Glisson's sheath of tumor-hosting separated liver lobe of the rat. At 40 min after contrast enhancement (**c**), with time, a progressively brightening and concentrically thickening rim occurred at the periphery of the RFA-induced necrotic lesion. Twenty-four hours after administration (within the broad imaging window from a few hours to a few days for any NACAs), ECIV-7 caused an atypical "O" type of CE pattern with a shape contouring the distal part of that liver lobe (**d**). The tumor as the core of this RFA-induced necrotic lesion was completely encompassed by a thick specifically enhanced rim composed of necrotic periphery, suggesting radical tumor ablation. These imaging findings matched perfectly with the gross section (**e**). *S* stomach

means ± standard deviations (SDs), and plotted as bar charts in function of time to compare between different tissue components. Statistical analysis was carried out with the SPSS for windows software package (release 10.0, SPSS, Chicago, Ill., USA). Paired and two-tailed Student's t-tests were applied for the comparisons of the contrast-enhancing properties of ECIV-7 between different tissue components at early and delayed phases. A difference was considered as significant if the P value was lower than 0.05.

Results

General aspects

All rats survived the procedures, including abdominal surgery for R1 implantation and real or sham RFA, and serial MRI under respective anesthetic regimes, without any observable side effects that could be related to injection of ECIV-7.

MRI findings

Before contrast enhancement The implanted intrahepatic R1 tumors appeared typically as well-demarcated hyperintense and slightly hypointense spheroid nodules on T2-w and T1-w MRI, respectively [21]. The RFA coagulated lesions varied from slightly hypointense to isointense relative to normal liver with or without a faint rim on T1-w images (Figs. 1a, 2a, 3a), which made lesion delineation and tissue characterization difficult.

Early after contrast enhancement Immediately after ECIV-7 administration the SI of normal liver was strongly enhanced (RE≈40–50%) and peaked 30 min later, leaving the
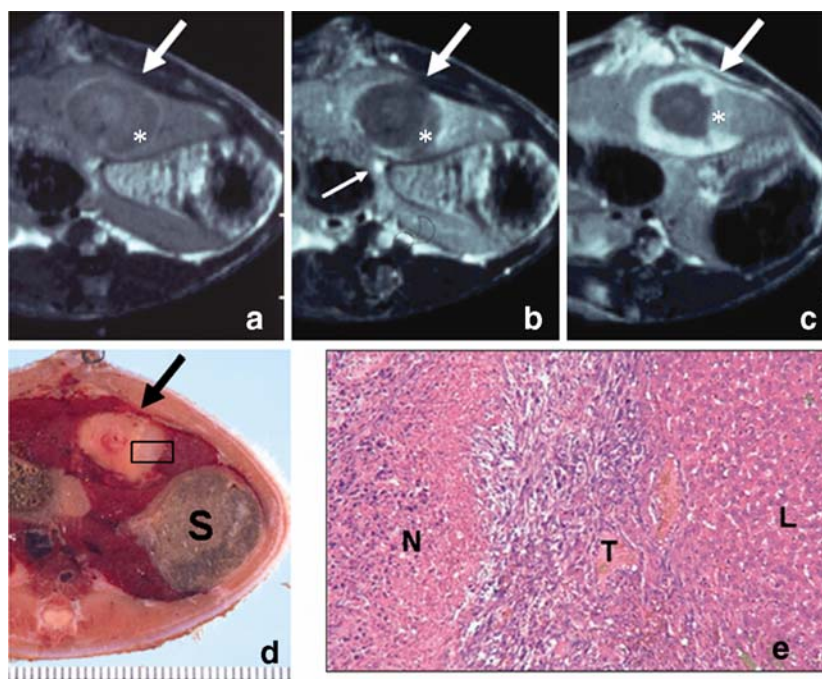
Fig. 3 T1-weighted TSE MR images **a** without and **b,c** with intravenous injection of a non-porphyrin NACA ECIV-7 at 0.05 mmol/kg. **d** corresponding macroscopic section and **e** photomicrograph from a group II rat with liver implantation of R1 tumor and 1 day after intended incomplete ablation of the tumor. While faintly discernible before contrast enhancement (**a**), the RFA lesion (*arrow*) was demarcated as a hypointense area 10 min after injection of ECIV-7 (**b**), due to strongly enhanced liver and slightly enhanced residual tumor (*asterisk*). Biliary contrast excretion was evident as strong CE at the common bile duct (*thin arrow*). Six hours after administration (within the broad imaging window from a few hours to a few days for any NACAs), ECIV-7 caused a typical "C" type of CE pattern and enabled the distinguishing of each tissue component with its characteristic contrast: a hypointense core of the ablated tumor, a strongly hyperintense horse-shoe sign of ablated margin, a moderately enhanced region of residual tumor at one end of the lesion, and liver parenchyma of almost normalized SI (**c**). These imaging findings matched perfectly with the gross section (**d**) and were further proven by histological findings (**e**) (hematoxylin–eosin, ×100). The rectangular frame across the transition zones in **d** approximates where the microscope (**e**) was focused, covering the pale coagulative tumor necrosis, the fish-flesh-like residual viable tumor, and normal liver parenchyma. At microscopy (**e**) the residual R1 tumor predominantly consisted of viable sarcoma cells with numerous mitoses, evident hypervasculature and enriched stromal matrices. While typical eosinophilic coagulation necrosis (*N*) occurred only at the borderline between the partially ablated and residual R1 tumor (*T*), the bulk thermal coagulation necrosis of the tumor and surrounding normal tissue appeared almost intact (further left on **e**, not shown) for their histomorphology, i.e., thermal fixation or "ghost" effect, due to preservation via heat-induced instantaneous denaturation of enzymatic proteins. *S* in **d** and *L* in **e** denote the stomach and normal liver, respectively

Fig. 4 Bar chart of RE of tissue components after the use of a necrosis-avid contrast agent in rats with implanted liver R1 tumor treated by RFA
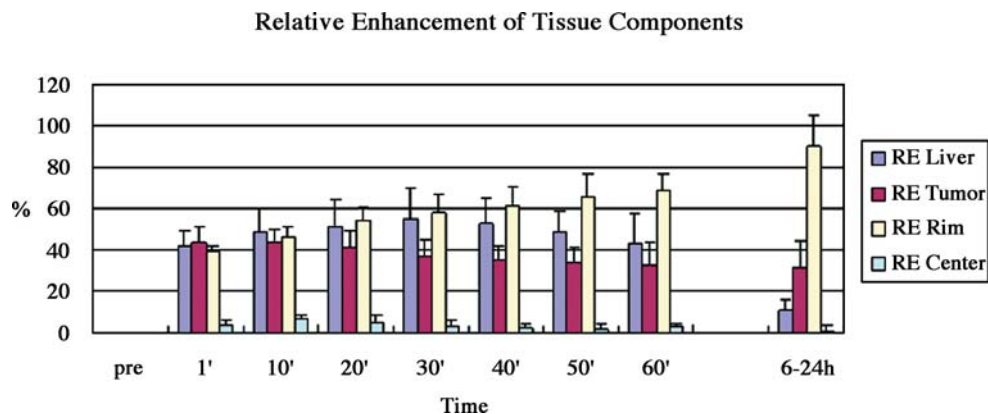
RFA lesion as a hypointense region or a negative lesion-over-liver CE in group I and group II (Figs. 1b, 2b, 3b). The liver CE decayed gradually afterwards. The SIs of the residual and intact tumors were also enhanced considerably in groups II and III and remained moderately elevated over a persistent period (RE≈30%). The discrepant SI levels of the liver and tumor caused a discernible tumor-to-liver negative CE (CR=0.86±0.05 at 30 min) during the first hour (Fig. 3b) [10]. While almost nothing was changed in the center of the RFA lesion (Figs. 1b,c, 2b,c, 3b), with time a peripheral rim occurred, with a progressively increasing SI and a concentrically broadening thickness (Figs. 1b,c, 2b,c, 3b). Therefore, except for the dark center of RFA lesions, visual contrasts between different enhancible tissue components varied or evolved in degrees and/or dimensions during the entire early post-contrast period (Figs. 1b,c, 2b,c, 3b, 4 and 5).

Delayed post-contrast phase Six to 24 hours after contrast enhancement, while liver SI declined to a low level (RE=11±5%) in all rats due to evident biliary excretion (Figs. 1c and 3b) [10], the SI of the extended peripheral zone had further increased to, and remained at, a strikingly high level (RE=90±15%). Consequently, two characteristic

CE patterns appeared (CR$_{rim/liver}$=1.89±0.09), i.e., the "O" type of hyperintense rim in group I, of complete tumor ablation (Fig. 1d), of which the shape could be non-spherical (Fig. 2d) due to the RFA "lobectomy" effect on the separated liver lobes in rats, and the "C" type of incomplete rim in group II, of incomplete tumor ablation (Fig. 3c) with its open gap being filled by moderately enhanced residual tumor (RE=31±13% and CR$_{tumor/liver}$≈ 1.2). As shown in Figs. 4 and 5, only at delayed phase, could tissues of different natures (viable versus non-viable and malignant versus benign) be specifically (in necrosis) or non-specifically (in viable tumor and liver) enhanced at discernable degrees, or simply unenhanced (in the coagulated center), altogether resulting in their visually appreciable contrasts (Figs. 1d, 2d, 3c) as quantified by significantly different RE values (P<0.05, Fig. 4) and discrete CRs (Fig. 5). The viable R1 tumors in groups II and III changed from hypointense before and during early contrast enhancement (Fig. 3a and b) to slightly hyper-intense during late contrast enhancement, due to non-specific uptake and retention of NACA (Fig. 3c) [10]. The results of statistical analysis of the RE of different tissue components and semiquantitative classification of CRs between adjacent tissues are summarized in Table 1.

Fig. 5 Bar chart of CRs between adjacent tissue components after the use of a necrosis-avid contrast agent in rats with implanted liver R1 tumor treated by RFA
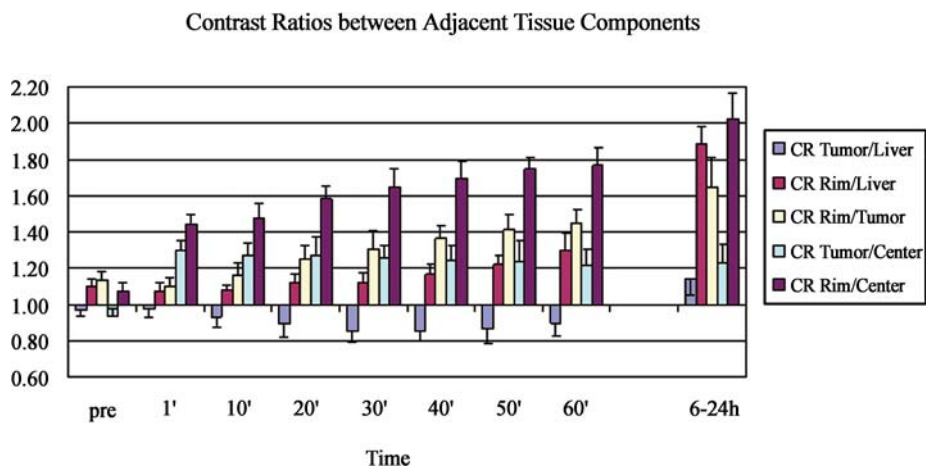
Table 1 Statistical results of relative enhancement and semi-quantitative classification of contrast ratios [*NA* not applicable, *NS* not statistically significant ($P>0.05$), *SS* statistically significant ($P<0.05$), *SPC* strong positive contrast ($CR\geq1.5$), *WNC* weak negative contrast ($0.8<CR<1.0$), *WPC* weak positive contrast ($1.0<CR<1.2$), *GPC* good positive contrast ($1.2\leq CR<1.5$)]

Timing		Before	1 min	10 min	20 min	30 min	40 min	50 min	60 min	6–24 h
RE	Liver–tumor	NA	NS	NS	NS	SS	SS	NS	NS	SS
	Rim–tumor	NA	NS	NS	SS	SS	SS	SS	SS	SS
	Rim–liver	NA	NS	NS	NS	NS	NS	SS	SS	SS
	Tumor–center	NA	SS	SS	SS	SS	SS	SS	SS	SS
	Rim–center	NA	SS	SS	SS	SS	SS	SS	SS	SS
	Liver–center	NA	SS	SS	SS	SS	SS	SS	SS	SS
CRs	Tumor/liver	WNC	WNC	WNC	WNC	WNC	WNC	WNC	WNC	WPC
	Rim/liver	WPC	WPC	WPC	WPC	WPC	WPC	GPC	GPC	SPC
	Rim/tumor	WPC	WPC	WPC	GPC	GPC	GPC	GPC	GPC	SPC
	Tumor/center	WNC	GPC	GPC	GPC	GPC	GPC	GPC	GPC	GPC
	Rim/center	WPC	GPC	GPC	SPC	SPC	SPC	SPC	SPC	SPC

Histomorphological findings

On gross section (Figs. 1e, 2e, 3d), in contrast to dark-red normal liver, the RFA-induced necrotic lesion appeared as well-demarcated pale regions without or with focal hemorrhage and small charred area around the needle track. The outlines of the central ablated tumor in the whole necrotic lesions were often recognizable (Fig. 2e), and a thin peri-ablational congestive rim was visible (Figs. 1e, 2e, 3d). The residual R1 tumor in group II (Fig. 3d) and the unablated R1 tumor in group III looked like fish flesh, with an expanding growth pattern [21]. The macroscopic view (Figs. 1e, 2e, 3d) matched perfectly with the MR images, even the fine details, e.g., NACA-enhanced rim corresponding to peripheral part of the necrotic lesions (Figs. 1d, 2d, 3c).

Microscopically, the residual and unablated R1 tumors in groups II and III consisted of predominantly viable sarcoma cells with numerous mitoses, evident hypervasculature and enriched stromal matrices (Fig. 3e), and no spontaneous necrosis had developed in this model when the tumor size was smaller than 10 mm [21]. A typical tumor RFA lesion contained, eccentrically, a vacuolated center of electrode track, a band of coagulated tumor, a zone of coagulated normal liver tissue as safety margin, and an outer layer of congestion and inflammation, altogether reflecting descending degrees of heat injury along the outward temperature gradient [1]. At microscopy, under hematoxylin–eosin (HE) staining, (Fig. 3e), while typical eosinophilic coagulation necrosis occurred only at the borderline between the ablated and residual R1 tumor, the bulky thermal coagulation necrosis of the tumor and surrounding normal tissue, which is characteristic of all acute thermal ablations [1], appeared almost intact (further left on Fig. 3e, not shown) in their histomorphology, due to preservation via heat-induced instantaneous denaturation of enzymatic proteins [1]. This phenomenon has been defined as thermal fixation or "ghost" effect in the literature [1, 26, 27].

Discussion

Despite the ever-increasing clinical application of various tumor ablation therapies, especially RFA with the achieved survival rate comparable to that of surgery [28], tumor relapse due to incomplete ablation still remains a critical issue and calls for the imaging modalities that enable determination of ablated area and identification of residual tumor tissue [1, 3]. However, so far, all efforts based on US, CT, and MRI have been unsuccessful, due to similar non-specific CE in the periphery of the ablation, which confuses residual tumor with benign peri-ablational hyperemic and regenerative tissues during the first 4 to 6 months after RFA [3–9].

More specific approaches, such as the use of macromolecular blood pool CA for MRI [7, 8] and functional ^{18}F-FDG positron computed tomography (PET) or hybrid PET-CT [3, 29], have been attempted to exploit, respectively, the hypervascular and hypermetabolic natures of malignant tumors. Although they were reportedly promising for the detection of residual tumor after RFA [7, 8, 30, 31], benign peri-ablational tissues share certain pathophysiological features with malignancies and, therefore, reveal similar imaging manifestations [9, 32, 33]. The reported sensitivity and accuracy for residual tumor detection were only at 65% and 68%, respectively, when ^{18}F-FDG PET or PET-CT were applied in clinic patients [29].

In comparison with the porphyrin NACAs such as Gadophrin-2, the non-porphyrin NACA ECIII-60 and ECIV-7 do not have dark colors and associated phototoxicity. They also demonstrated higher necrosis avidity by revealing simultaneous T1 and T2 dual CE of acute myocardial infarction, even at a low dose of 50 μmol/kg [10]. This is caused primarily by preferential accumulation of these NACA chelates in the necrotic spots, as proven by very high local gadolinium concentrations during delayed phase and, secondarily, by the augmented relaxivities due to

NACA–substrate interactions [10, 24]. Besides such necrosis-avid property, all NACAs also present other less specific functions, as seen with EFS, blood pool and hepatobiliary CAs, especially during the early postcontrast phase when most dynamic drug distribution, circulation and excretion occur [10, 19]. All these specific and non-specific functions with NACAs could well be exploited for solving the problems addressed by this study.

As demonstrated in the present CE-MRI study, the non-porphyrin NACA ECIV-7 was able to specifically label necrotic tissues and non-specifically enhance viable liver and tumor tissues, with all having their own maximum levels at different optimum time points. Thus, these tissue components could be visually stratified, even as early as 1 day after RFA, as opposed to a few months of waiting time when the EFS CAs were used, which carries a high risk of tumor regional invasion and remote metastases [4, 5, 6]. Furthermore, arguing whether residual tumor can be differentiated from benign peri-ablational "enhancement" by using other less specific imaging agents would no longer be necessary if the present method were to be applied [3, 7–9, 30–33]. The comparative results between MRI and histomorphology suggest that such a novel application of NACAs might prove to be a virtual biopsy technique with an in vivo effect of histochemical staining. Though NACAs are not yet available, their unprecedented competence should warrant further preclinical and clinical development [10].

Early phase manifestations Immediately after intravenous administration, the NACA, as a small molecular CA with and/or without protein binding, underwent intravascular perfusion, extravasation, interstitial diffusion, intracellular uptake by hepatocytes to a greater extent and by other parenchymal cells (both malignant and benign) to a lesser extent, and subsequent hepatobiliary and urinary excretion [10]. Such relatively less specific activities resulted, predominantly, in negative CE or "filling defect" sign of the RFA lesion in groups I and II, similar to the first postcontrast images when the EFS CAs were used at all modalities [3–6]. Stronger and faster hepatobiliary CE also made the intact R1 tumors in group III more conspicuous shortly after NACA administration [10], a contrast effect revealed by other typical hepatobiliary CAs such Mn-DPDP and Gd-EOB-DTPA [10, 34]. Meanwhile, starting at the vicinity of functioning blood vessels at the periphery of RFA lesions, specific interactions of the NACA with the exposed and denatured life molecules as a common consequence of all virtually ablative therapies took place. Driven by the concentration gradient of the NACA, this process continued with in-depth molecular diffusion, causing an evolving rim CE. In addition, the CE appearance with ECIV-7 at approximately 30 min after contrast enhancement differed visually, both in degree and extent, from the delayed rim CE with the non-specific EFS or blood pool CAs [3–9].

Delayed phase performance Vascular shutdown has been found to be one of the most prominent tumoricidal effects of RFA [1, 27], which limits the diffusing access of the NACA throughout the entire RFA-induced necrotic lesion, especially at the central part when the lesion size is over 1 cm; hence, there is only rim CE, similar to that seen with occlusive myocardial infarction [13, 18]. Being facilitated by peripheral blood perfusion, in-depth diffusion and chemotactic interactions over a time window matching the relatively long plasma half life, the gradually formed persistent striking rim CE (CR>1.5) appears characteristic only in NACAs, but not any other CAs [1, 10], which can be utilized for resolving the issue of tissue viability. The revealed "O" or "C" type of rim CE may help to determine whether complete or incomplete tumor RFA could have been achieved. While the non-specific perfusion and diffusion at peri-ablational tissues during the early postcontrast phase have disappeared and the less specific CE of peri-ablational hepatocytes and/or inflammatory cells becomes diminished with time, the residual tumor with mildly elevated SI can be easily identified. Thus, the issue of "differentiating benign peri-ablational enhancement from residual tumor" may thus be resolved [7–9]. The observed minimal but persistent tumoral CE can be explained mainly by the non-specific uptake of the NACA (being mistaken as a chemical metabolite) by the tumoral cells and a lack of biliary excretion mechanism in the tumor, and, to a lesser extent, by the minute specific binding of the NACA to the stromal matrices existing in the tumor. This could be part of the reason why some porphyrin and non-porphyrin derivatives had been regarded as tumor-specific sensitizers for cancer photodynamic therapy or tumor-seeking CAs for MRI [10]. The real targets of these compounds have recently been shifting from the previously believed tumor parenchyma to recently recognized tumor stroma [35–37], a contentious mechanism proposed over 10 years ago [10].

The liver is the most common organ harboring primary and secondary malignancies and most frequently studied for virtual ablative therapies [1]. Unlike other animal studies that recruited subcutaneously or intramuscularly implanted tumor models [7], our experiment, by using the R1 liver tumor model, could provide more clinically relevant information. Compared with that in the muscle, CE patterns after tumor ablation therapies can largely differ in the liver because of its abundant vasculature, distinct hemodynamics and unique microenvironment [9]. This, together with the mix of specific and non-specific CE patterns, could explain the previously reported, somewhat incomprehensible, results using a porphyrin NACA, Gadophrin-2, in rabbits with intramuscular implantation of VX2 carcinoma [9, 38, 39]. Therefore, once the correct methodologies are adopted, the resultant imaging outcomes with NACAs have always been reproducible in terms of the unambiguous necrosis-specific CE [10–25].

Despite the demonstrated excellent multifunctional performances of the NACAs, particularly with the non-

porphyrin species, the research in this direction has been slow. Elucidation of the mechanisms of action behind the unique effects of NACAs appears most critical for further preclinical and clinical development of this unique targeting and multipurpose approach [10, 37].

There exist some limitations in the present study and in the potential future applications of NACAs. Firstly, it is impossible to make definite therapeutic assessment during the RFA procedure due to the time consuming pharmacodynamic process of NACAs interacting with necrotic lesions. Therefore, a second RFA session seems unavoidable if any residual tumor can be detected on delayed NACA-enhanced MRI. Secondly, biphasic MRI at early and overnight delayed postcontrast phases appears necessary for comprehensive evaluation of both non-specific and specific CE of the target lesion, which can be impractical and costly. Alternatively, two approaches can be considered in clinical practice: either to combine precontrast baseline and both early and delayed postcontrast MRI for a comprehensive therapeutic assessment, which, though, is more expensive and time-consuming but with more information about early perfusion and non-specific contrast uptake, or to inject a NACA in advance and perform only delayed postcontrast MRI a few hours or overnight afterwards, since such delayed phase MRI proved indispensable for visualizing both necrosis-specific CE on ablated lesions and faint contrast retention on residual tumors or for more specific tissue characterization, and can be more economical and straight-forward.

In summary, NACA-enhanced MRI was able to determine the ablated area and to identify residual tumor after RFA in this animal study. More intensive experimental research is necessary before this approach may eventually benefit clinical patients for assuring higher cure rates of solid tumors with various tumor ablation techniques.

Reference

1. Ni Y, Mulier S, Miao Y, Michel L, Marchal G (2005) A review of the general aspects of radiofrequency ablation. Abdom Imaging 30:381–400
2. Hynynen K, McDannold N (2004) MRI guided and monitored focused ultrasound thermal ablation methods: a review of progress. Int J Hyperthermia. 20:725–737
3. Antoch G, Vogt FM, 4 P, Freudenberg LS, Blechschmid N, Dirsch O, Bockisch A, Forsting M, Debatin JF, Kuehl H (2005) Assessment of liver tissue after radiofrequency ablation: findings with different imaging procedures. J Nucl Med 46:520–525
4. Dromain C, de Baere T, Elias D, Kuoch V, Ducreux M, Boige V, Petrow P, Roche A, Sigal R (2002) Hepatic tumors treated with percutaneous radiofrequency ablation: CT and MR imaging follow-up. Radiology 223:255–262
5. Tsuda M, Majima K, Yamada T, Saitou H, Ishibashi T, Takahashi S (2001) Hepatocellular carcinoma after radiofrequency ablation therapy: dynamic CT evaluation of treatment. Clin Imaging. 25:409–415
6. Bartolozzi C, Crocetti L, Cioni D, Donati FM, Lencioni R (2001) Assessment of therapeutic effect of liver tumor ablation procedures. Hepatogastroenterology. 48:352–358

7. Kim TJ, Moon WK, Cha JH, et al (2005) VX2 carcinoma in rabbits after radiofrequency ablation: Comparison of MR contrast agents for help in differentiating benign periablational enhancement from residual tumor. Radiology 234:423–430
8. Goldberg SN (2005) Can we differentiate residual untreated tumor from tissue responses to heat following thermal tumor ablation? Radiology 234:317–318
9. Ni Y, Chen F, Marchal G (2005) Differentiation of residual tumor from benign periablational tissues after radiofrequency ablation: the role of MRI contrast agents (letter). Radiology 237:745–749
10. Ni Y, Bormans G, Chen F, Verbruggen A, Marchal G (2005) Necrosis avid contrast agents: functional similarity versus structural diversity (review). Invest Radiol 40:526–535
11. Marchal G, Ni Y, Herijgers P, Flameng W, Petré C, Bosmans H, Yu J, Ebert W, Hilger CS, Pfefferer D, Semmler W, Baert AL (1996) Paramagnetic metalloporphyrins: infarct avid contrast agents for diagnosis of acute myocardial infarction by magnetic resonance imaging. Eur Radiol 6:1–8
12. Ni Y, Marchal G, Herijgers P, et al (1996) Paramagnetic metalloporphyrins: from enhancers for malignant tumors to markers of myocardial infarcts. Acad Radiol 3:S395–S397

13. Ni Y (1998) Myocardial viability. In: Bogaert J, Duerinckx AL, Rademakers FE (eds) Magnetic resonance of the heart and great vessels: clinical applications, 1st edn, Springer, Berlin Heidelberg New York, pp 113–132
14. Pislaru S, Ni Y, Pislaru C, Bosmans H, Miao Y, Bogaert J, Semmler W, Marchal G, Van de Werf F (1999) Noninvasive measurements of infarct size after thrombolysis with a necrosis-avid MRI contrast agent. Circulation 99:690–696
15. Choi SI, Choi SH, Kim ST, Lim KH, Lim CH, Gong GY, Kim HY, Weinmann HJ, Lim TH (2000) Irreversibly damaged myocardium at MR imaging with a necrotic tissue-specific contrast agent in a cat model. Radiology 215:863–868
16. Ni Y, Pislaru C, Bosmans H, Pislaru S, Miao Y, Bogaert J, Dymarkowski S, Yu J, Semmler W, Van de Werf F, Baert AL, Marchal G (2001) Intracoronary delivery of Gd-DTPA and Gadophrin-2 for determination of myocardial viability with MR imaging. Eur Radiol 11:876–883
17. Saeed M, Lund G, Wendland MF, et al (2001) Magnetic resonance characterization of the peri-infarction zone of reperfused myocardial infarction with necrosis-specific and extracellular non-specific contrast media. Circulation 103:871–876

18. Ni Y, Dymarkowski S, Chen F, Bogaert J, and Marchal G (2002) Occlusive myocardial infarction: enhanced or not enhanced with necrosis avid contrast agents at magnetic resonance imaging. Radiology 225:603–605

19. Ni Y, Cresens E, Adriaens P, Dymarkowski S, Bogaert J, Zhang H, Bosmans H, Verbruggen A, Marchal G (2002) Exploring multifunctional features of necrosis avid contrast agents. Acad Radiol 9 [Suppl 2]:S488–S490

20. Hermens AF, Barendsen GW (1967) Cellular proliferation patterns in an experimental rhabdomyosarcoma in the rat. Eur J Cancer 3:361–369

21. Chen F, Sun X, De Keyzer F, Yu J, Peeters R, Coudyzer W, Vandecaveye V, Bosmans H, Van Hecke P, Landuyt W, Hermans R, Marchal G, Ni Y (2005) A rodent liver tumor model with implanted rhabdomyosarcoma: characterization using magnetic resonance, microangiography and histopathology. Radiology (in press)

22. Cresens E, Ni Y, Adriaens P, Verbruggen A, Marchal G (2001) Substituted bis-indole derivatives useful as contrast agents, pharmaceutical compositions containing them and intermediates for producing them. International Patent Application PCT/BE01/00192 (7 November 2001)

23. Marchal G, Verbruggen A, Ni Y, Adriaens P, Cresens E (1999) Non-porphyrin compounds for use as a diagnosticum and/or pharmaceutical. International Patent Application PTC/BE99/00104 (5 August 1999)

24. Ni Y, Petré C, Miao Y, et al (1997) Magnetic resonance imaging—histomorphologic correlation studies on paramagnetic metalloporphyrins in rat models of necrosis. Invest Radiol 32:770–779

25. Ni Y, Adzamli K, Miao Y, et al (2001) MRI contrast enhancement of necrosis by MP-2269 and Gadophrin-2 in a rat model of liver infarction. Invest Radiol 36:97–103

26. Coad JE, Kosari K, Humar A, Sielaff TD (2003) Radiofrequency ablation causes thermal fixation of hepatocellular carcinoma: a post-liver transplant histopathologic study. Clin Transpl 17:377–384

27. Miao Y, Ni Y, Mulier S, et al (2000) Treatment of VX2 liver tumor in rabbits with "wet" electrode mediated radiofrequency ablation. Eur Radiol 10:188–194

28. Solbiati L, Livraghi T, Goldberg SN, et al (2001) Percutaneous radio-frequency ablation of hepatic metastases from colorectal cancer: long-term results in 117 patients. Radiology. 221:159–166

29. Veit P, Antoch G, Stergar H, Bockisch A, Forsting M, Kuehl H (2005) Detection of residual tumor after radiofrequency ablation of liver metastasis with dual-modality PET/CT: initial results. Eur Radiol (in press), 2005 May 3 [Epub ahead of print]

30. Langenhoff BS, Oyen WJ, Jager GJ, et al (2002) Efficacy of fluorine-18-deoxyglucose positron emission tomography in detecting tumor recurrence after local ablative therapy for liver metastases: a prospective study. J Clin Oncol. 20:4453–4458

31. Anderson GS, Brinkmann F, Soulen MC, Alavi A, Zhuang H (2003) FDG positron emission tomography in the surveillance of hepatic tumors treated with radiofrequency ablation. Clin Nucl Med 28:192–197

32. Shreve PD, Anzai Y, Wahl RL (1999) Pitfalls in oncologic diagnosis with FDG PET imaging: physiologic and benign variants. Radiographics 19: 61–77

33. Cook GJ, Maisey MN, Fogelman I (1999) Normal variants, artefacts and interpretative pitfalls in PET imaging with 18-fluoro-2-deoxyglucose and carbon-11 methionine. Eur J Nucl Med. 26:1363–1378

34. Ni Y, Marchal G (1998) Enhanced magnetic resonance imaging for tissue characterization of liver abnormalities with hepatobiliary contrast agents: an overview of preclinical animal experiments (review). Top Magn Reson Imaging 9:183–195

35. Peng Q, Nesland JM (2004) Effects of photodynamic therapy on tumor stroma. Ultrastruct Pathol 28:333–340

36. Van de Putte M, Roskams T, Vandenheede JR, Agostinis P, de Witte PA (2005) Elucidation of the tumori-tropic principle of hypericin. Br J Cancer 92:1406–1413

37. Ni Y, Chen F, Bormans G, Verbruggen A, Marchal G (2005) Targeting stroma: natural mechanisms derived from photodynamic therapy (PDT) and necrosis avid contrast agents (NACAs)? Mol Imaging 4:382 (abstract ID 556)

38. Kim TK, Choi BI, Park SW, Lee W, Han JK, Han MC, Weinmann HJ (2000) Gadolinium mesoporphyrin as an MR imaging contrast agent in the evaluation of tumors: an experimental model of VX2 carcinoma in rabbits. AJR Am J Roentgenol 175: 227–234

39. Ju Lee H, Kim IO, Kim TK, Hyung Kim S, Choi JI, Woo Lee J, Kyung Moon W, Choi BI, Chung Han M, Weinmann HJ, Hyun Chang K (2002) Dynamic enhancement features of gadophrin-2 on magnetic resonance imaging: an experimental model of VX2 carcinoma and bacterial abscess in rabbit thigh. Invest Radiol 37:663–671